Streamwise inclination angle of large wall-attached structures in turbulent boundary layers

Rahul Deshpande[1],†, **Jason P. Monty**[1] **and Ivan Marusic**[1]

[1]Department of Mechanical Engineering, University of Melbourne, Parkville, VIC 3010, Australia

(Received 17 May 2019; revised 29 July 2019; accepted 8 August 2019)

The streamwise inclination angle of large wall-attached structures, in the log region of a canonical turbulent boundary layer, is estimated via spectral coherence analysis, and is found to be approximately 45°. This is consistent with assumptions used in prior attached eddy model-based simulations. Given that the inclination angle obtained via standard two-point correlations is influenced by the range of scales in the turbulent flow (Marusic, *Phys. Fluids*, vol. 13 (3), 2001, pp. 735–743), the present result is obtained by isolating the large wall-attached structures from the rest of the turbulence. This is achieved by introducing a spanwise offset between two hot-wire probes, synchronously measuring the streamwise velocity at a near-wall and log-region reference location, to assess the wall coherence. The methodology is shown to be effective by applying it to data sets across Reynolds numbers, $Re_\tau \sim O(10^3)$–$O(10^6)$.

Key words: boundary layer structure, turbulent boundary layers, turbulence modelling

1. Introduction

The turbulent boundary layer (TBL) consists of an ensemble of coherent motions (Robinson 1991) which are responsible for the production and dissipation of turbulence. Previous studies have found the majority of these motions to be inclined forwards in the direction of the mean flow. Table 1 lists a small selection of the many studies that have reported the streamwise inclination angle (θ) of these motions in a zero pressure gradient (ZPG) TBL at various Reynolds numbers. As is evident from the table, the value of θ varies significantly depending on the type of structure it is defined for, with subscripts 'm' and 's' referring to inclination angle of a mean and individual flow structure, respectively (terminology inspired from Adrian, Meinhart & Tomkins (2000), who also noted this difference). The superscript 'w' is considered when referring to wall-attached structures only. Throughout this article, the words 'motions', 'structures' and 'eddies' are used interchangeably, and essentially follow the definition of a coherent motion given by Robinson (1991).

† Email address for correspondence: raadeshpande@gmail.com

θ_s in the outer region of wall-bounded flow			θ_s^w assumed for AEH simulations		θ_m^w in the log region of wall-bounded flow		
Reference	Re_θ	θ_s	Reference	θ_s^w	Reference	Re_τ	θ_m^w
Head & Bandyopadhyay (1981)	500–10 000	45°	Perry & Marusic (1995)	45°	Brown & Thomas (1977)	3413	18°
Moin & Kim (1985)[a]	13 800	45°	Baidya *et al.* (2014, 2017)	45°	Marusic & Heuer (2007)	1350	14°
Adrian *et al.* (2000)	930–6845	3°–35°	Chandran *et al.* (2017)	45°	Marusic & Heuer (2007)[b]	1.4×10^6	14°

TABLE 1. A summary of the streamwise inclination angles (θ) of coherent motions in a ZPG TBL, estimated (θ_s, θ_m^w) or assumed (θ_s^w) in various studies. Friction Reynolds number, Re_τ, is defined based on friction velocity (u_τ) and TBL thickness (δ), whereas Re_θ is based on free-stream velocity (U_∞) and momentum thickness (θ). Terminology for angles has been described in § 1.

[a]This study was for a fully developed turbulent channel flow and their Reynolds number is defined based on channel centreline velocity and half-width.
[b]Results are for atmospheric surface layer under neutrally buoyant conditions.

The information on the structure inclination angle is important from a wall-turbulence modeller's perspective, be it developing a model of the near-wall region for a large eddy simulation (LES; Piomelli & Balaras 2002) or to predict the TBL velocity statistics by modelling the flow based on the attached eddy hypothesis (AEH; Marusic & Monty 2019). The latter approach has gained popularity for investigating the kinematics in the logarithmic (log) region of a TBL by representing it with an assemblage of self-similar wall-attached vortex structures. Researchers who have utilized the AEH approach previously (table 1) assumed θ_s^w for these statistically representative structures to be equivalent to θ_s recorded by identifying structures via flow visualization, vortex identification techniques, and so on. Here θ_s estimated in these studies, however, was based on structures clearly discernible only in the outer region of the boundary layer (Moin & Kim 1985), with no evidence of these being wall-coherent (hence not referred here as θ_s^w). Notwithstanding, the AEH simulations yield results consistent with experimental observations, suggesting $\theta_s^w \approx 45°$ is a good assumption. Theoretical support towards θ_s^w being nominally 45° is obtained on investigating the mean-strain-rate and rotation tensor, the two components of the velocity gradient tensor, for a ZPG TBL which is two-dimensional in the mean. As pointed out by Moin & Kim (1985) and Perry, Uddin & Marusic (1992), it is more likely for eddies in such a flow to assume the direction of the principal rate of mean strain since the rotation field has no preferred direction. If we consider ψ to correspond to the inclination of the principal rate of mean strain with the streamwise direction (x) and z to be the wall-normal direction, it was deduced by Perry *et al.* (1992) that

$$\psi = \frac{1}{2}\text{atan}\left(\frac{\dfrac{\partial U}{\partial z}}{2\dfrac{\partial U}{\partial x}}\right), \tag{1.1}$$

from which $\psi = 45°$ for a ZPG TBL, where $\partial U/\partial x = 0$, with U being the mean streamwise velocity. In spite of these arguments, there is still a lack of empirical evidence to support the claim of $\theta_s^w \approx 45°$.

Apart from direct visualization of individual structures, experimentalists (table 1) have statistically estimated the inclination angle of a mean wall-attached structure (θ_m^w) in the log region via cross-correlating simultaneously acquired wall shear stress (τ) and velocity (u) fluctuations. This is achieved through probes on the wall ($z = 0$) and in the log region ($z = z_o$), respectively following

$$R_{\tau u}(\Delta t) = \frac{\langle \tau(t) u(z_o;\, t + \Delta t)\rangle}{\sqrt{\langle \tau^2\rangle}\sqrt{\langle u^2(z_o)\rangle}}, \tag{1.2}$$

where angle brackets ($\langle\,\rangle$) denote the ensemble time average, with t being the time. Here, u, v and w refer to the streamwise, spanwise and wall-normal velocity fluctuations, respectively, associated with the coordinate system x, y and z. To estimate θ_m^w, the temporal delay (Δt_p) corresponding to the peak in $R_{\tau u}$ is identified (Marusic & Heuer 2007) and then $\theta_m^w = \text{atan}(z_o/(\Delta t_p U_c))$, where U_c is the convection velocity. The stark difference between θ_m^w and the expected θ_s^w exists due to θ_m^w being a function of the distribution and the range of scales of eddies convecting past the two probes (Marusic 2001); hence, giving it the name of a mean structure angle (figure 1 differentiates θ_m^w and θ_s^w; see also figure 13 in Head & Bandyopadhyay 1981). Marusic (2001) demonstrated this via attached eddy simulations by considering individual eddies (with $\theta_s^w \approx 45°$) of various length scales in an organized manner, analogous to a spatially correlated packet of vortices observed experimentally by Adrian *et al.* (2000). It was shown that θ_m, estimated from the cross-correlations obtained from these simulated fields, closely resembles the experimentally obtained inclination angles. On the other hand, it was found that $\theta_m \approx \theta_s$ when eddies of only specific length scales were considered in the simulation. In a real turbulent boundary layer experiment, it is possible to isolate structures of specific length scale from the rest in post-processing. In the present study, we draw inspiration from the recent work of Baidya *et al.* (2019) to isolate large wall-attached structures in a TBL by imposing a spanwise offset between the log-region and wall probe to find θ_s^w.

2. Methodology adopted to isolate large wall-attached structures

We begin by demonstrating the methodology adopted to isolate large wall-attached structures via a conceptual reconstruction of a TBL from an AEH view point. Figure 1(*a–c*) shows a schematic with a hierarchy of self-similar wall-attached structures representing the log region of a TBL (Baidya *et al.* 2019; Marusic & Monty 2019). Apart from these preferentially forward-inclined structures, which represent the majority, a real TBL will invariably also consist of additional randomly oriented structures (Perry *et al.* 1992) that influence the flow statistics. These, however, are not considered in AEH-based simulations. Here, four hierarchy levels of randomly positioned attached eddies are considered, with each hierarchy shown in a different colour. Starting from the hierarchy with the smallest eddies (yellow), the eddy size in each consecutive hierarchy is doubled in a self-similar manner and the number of eddies is quartered in three-dimensional space. For simplicity, we consider the volume of influence of eddies, in each level, to be characterized by $\mathcal{L}_i$, $\mathcal{W}_i$ and $\mathcal{H}_i$ in the x, y and z directions, respectively, with $i = 1$–4 denoting the hierarchy level. A spectral analysis of the flow field consisting of such eddies would lead to their

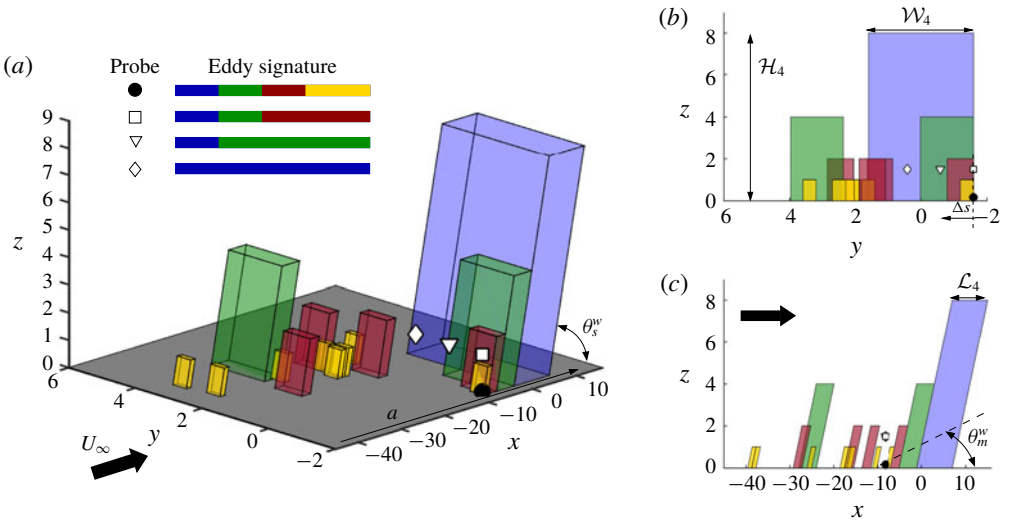

FIGURE 1. Schematic showing the (*a*) isometric, (*b*) *y*–*z* plane and (*c*) *x*–*z* plane view of a hierarchy of self-similar wall-attached eddies representing the log region of a ZPG TBL shown as simplified cuboids. Four hierarchy levels are considered, each represented by different colours. Symbols represent various probe locations. Eddy signatures identified by respective probes, over a streamwise distance of a, are shown in (*a*). Here L_i, W_i and H_i denote the streamwise, spanwise and wall-normal extent of a hierarchy level; θ_m^w and θ_s^w denote mean and individual structure angles, respectively. Figure concept adopted from Baidya *et al.* (2019).

lengths and spans showing up as wavelengths, $\lambda_x \sim 2\mathcal{L}_i$ and $\lambda_y \sim 2\mathcal{W}_i$ (Baidya *et al.* 2019). Here, $\lambda_x = 2\pi/k_x$ where k_x is the streamwise wavenumber. θ_s^w represents the streamwise inclination of the individual eddies.

The solid and empty symbols represent probes placed on the wall and in the log region, respectively, to synchronously record the signature of the convecting eddies, shown in figure 1(*a*). The □ probe is able to record all except the smallest hierarchy in comparison to the wall probe (●). Accordingly, the correlation between u fluctuations from □ and ● probes (following (1.2)) represents a mean structure of the wall-attached flow influenced by the hierarchy levels 2, 3 and 4 (Marusic 2001). The inclination angle of this mean structure is given by θ_m^w (figure 1*c*). Increasing the relative spanwise offset (Δs) between the log-region and wall probes means that only the hierarchy levels with the large eddies correlate between the two probes. For example, considering probe ◇ placed at $W_3 < \Delta s < W_4$, only eddies belonging to the fourth hierarchy remain correlated with the wall probe, effectively isolating these eddies from the others. Following Marusic (2001), we hypothesize that the streamwise inclination angle obtained on correlating the u fluctuations from ● and ◇ probes should reflect the angle for a large individual wall-attached structure θ_s^w in this simplified flow model. We consider experimental as well as numerical data sets which allow us to work along this hypothesis in the following sections. It is to be noted that the relative offset, Δs, can be obtained on moving either the log-region or wall probe along y, owing to the spanwise homogeneity of the TBL.

Data set:			
Label	$\mathcal{S}_1$	$\mathcal{E}_1$	$\mathcal{E}_2$
Facility	DNS (raw)	HRNBLWT	SLTEST atm.
Study	Sillero *et al.* (2013)	Present study	Hutchins *et al.* (2012)
$Re_\tau \approx$	2000	14 000	7.7×10^5
Near-wall sensor:			
Sensor	—	Hot-wire	Sonic
$z_r^+ \approx$	14.6	15	$0.036Re_\tau$
$\Delta y^+ \approx$	3.7	22	1000
Log-region sensor:			
Sensor	—	Hot-wire	Sonic
$z_o^+ \approx$	$2.6\sqrt{Re_\tau}$	$2.6\sqrt{Re_\tau}$, $3.9\sqrt{Re_\tau}$	$0.05Re_\tau$
$\Delta y^+ \approx$	3.7	22	1000
$\Delta s/\delta \approx$	0.00–0.15	0.00–0.15	0.00–0.15

TABLE 2. A summary of the various data sets containing synchronized multi-point measurements at a near-wall (z_r) and log-region (z_o) reference location at various spanwise offsets, Δs. Here Δy^+ represents the spatial resolution of the sensor/grid along the spanwise direction. DNS, direct numerical simulation; SLTEST, Surface Layer Turbulence and Environmental Science Test.

3. Experimental and numerical data

To test the hypothesis proposed in the previous section, we consider three data sets (table 2), each comprising synchronized two-point u velocity signals at a near-wall (z_r) and a log-region (z_o) reference location for various spanwise offsets, Δs. One of these is the DNS by Sillero, Jiménez & Moser (2013) ($\mathcal{S}_1$). Thirteen raw DNS time blocks, spanning up to 11.9δ in x, were considered such that the Reynolds number increases nominally across the domain. This is the same block size considered by Baars, Hutchins & Marusic (2017) for their linear coherence spectrum (LCS) analysis with $Re_\tau \approx 1992$ at the streamwise centre of the domain. Here, values of δ for both data sets $\mathcal{S}_1$ and $\mathcal{E}_1$ were calculated by a modified Coles law of the wake fit (Jones, Marusic & Perry 2001). Both z_r^+ and z_o^+ (viscous-scaled) in $\mathcal{S}_1$ were chosen to correspond with the experimental data set, $\mathcal{E}_1$ (described next).

The high-Re_τ laboratory measurements ($\mathcal{E}_1$) were conducted in the large Melbourne wind tunnel (HRNBLWT). They were made possible by employing the same experimental set-up used by Chandran *et al.* (2017). Figure 2(*a*) shows a schematic of how the experiment was conducted. The set-up comprised of two 2.5 μm diameter Wollaston hot-wire probes – HW_r and HW_o at wall-normal heights z_r and z_o, respectively. They were operated using an in-house Melbourne University Constant Temperature Anemometer (MUCTA) at a viscous-scaled sampling rate ∼0.5. The same calibration procedure, as employed by Chandran *et al.* (2017), was followed, wherein the HW_o was calibrated in the TBL using the free-stream-calibrated HW_r as a reference. The measurement began with both probes vertically aligned (figure 2*a*i), which was ensured by viewing the arrangement via a traversable microscope. Long velocity signals were acquired with a length of $TU_\infty/\delta \approx 20\,000$ (T is the total sampling duration) to obtain converged statistics at the largest energetic wavelengths. As the experiment progressed, HW_r always remained at a fixed spanwise location while HW_o was traversed in the spanwise direction (with log spacing) as shown in

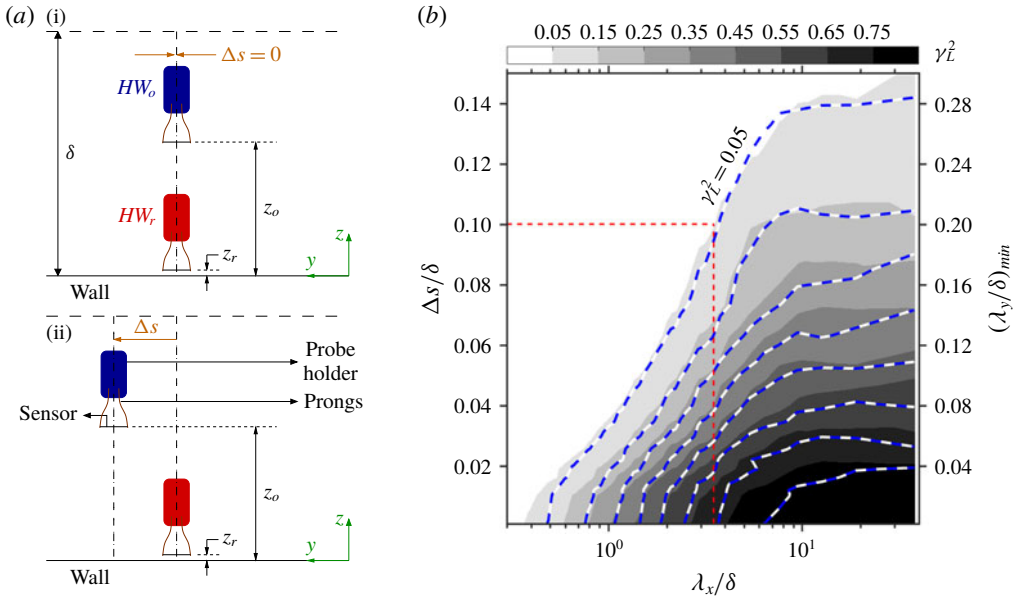

FIGURE 2. (*a*) Schematic of the experimental set-up in HRNBLWT showing locations of the near-wall (HW_r) and log-region (HW_o) reference probe. Mean flow direction is along x. The experiment begins with HW_o placed vertically above HW_r ($\Delta s = 0$; i) and is followed by the spanwise traverse ($\Delta s > 0$; ii) of HW_o. (*b*) γ_L^2 computed as a function of λ_x and Δs on correlating u from HW_o and HW_r for data set $\mathcal{E}_1$. The grey scale and line contours correspond to γ_L^2 for $z_o^+ \approx 2.6\sqrt{Re_\tau}$ and $3.9\sqrt{Re_\tau}$, respectively. Both contours are at levels $0.05 : 0.1 : 0.85$. The red dashed line is used to highlight the streamwise spectral cutoff $\lambda_{x,c}$ corresponding to $\Delta s/\delta = 0.1$.

figure 2(*a*ii). HW_o was traversed only up to $\Delta s/\delta \approx 0.15$ since the cross-correlation tends to 0 at such spans (Baidya *et al.* 2019). Although the present study focuses on inclination angles of wall-attached structures, a hot-wire probe positioned at $z_r^+ \approx 15$ was preferred over a wall-mounted shear stress sensor (hot-film) owing to spatial resolution and frequency response issues (Baars *et al.* 2017). This was possible due to the observation made by Baars *et al.* (2017) on the wall-coherence analysis being unaffected for $0 < z_r^+ \lesssim 15$. The data set $\mathcal{E}_1$ consists of two cases of z_o^+ (table 2), both lying within the log region of the TBL (Baars *et al.* 2017).

The data set at the highest Reynolds number, $Re_\tau \approx 7.7 \times 10^5$ ($\mathcal{E}_2$), consists of one hour of synchronously acquired u fluctuations in the atmospheric surface layer (under near-neutral buoyant conditions) by a spanwise and wall-normal array of 18 sonic anemometers at the SLTEST facility. Here, we consider the sonic anemometers located at 4.26 m from the ground (*t*4; refer figure 1 of Hutchins *et al.* 2012) as the log-region reference. Of the 10 sonic anemometers in the spanwise array, each of which were separated by approximately 3 m and fixed at approximately 2.14 m from ground, we consider only four sonic anemometers (*s*1–*s*4) to obtain relative spanwise offsets, $0 \lesssim \Delta s/\delta \lesssim 0.15$ ($\delta = 60$ m for $\mathcal{E}_2$) and to act as the near-wall reference. Given that z_r is significantly far from the wall, the structure inclination angle obtained through data set $\mathcal{E}_2$ cannot be associated with a wall-attached structure. This data set is used here merely to demonstrate the feasibility of isolating large structures by introduction of a spanwise offset between the two reference probes. For the case of both temporal

data sets $\mathcal{E}_1$ and $\mathcal{E}_2$, Taylor's frozen turbulence hypothesis is used to construct cross-correlation functions between z_o and z_r, at different streamwise (Δx) spacings, by assuming the local mean velocity at z_o (that is, $U(z_o)$) to be the convection speed (U_c) of the flow structures (Baars *et al.* 2017). We expect the effects due to this assumption to be minimal since the present analysis is restricted to the log region, where this assumption has been shown to perform reasonably well for estimating streamwise velocity correlations (Uddin 1994; de Silva *et al.* 2015). Further, as noted by Alving, Smits & Watmuff (1990), even the choice of U_c does not significantly influence the estimation of the structure inclination angle.

4. Results and discussions

4.1. *Variation in scale-specific wall coherence with spanwise offset*

Quantitative support towards the idea of isolating large wall-attached structures in the log region (proposed in § 2) should come by analysing the one-dimensional LCS (Baars *et al.* 2017; Baidya *et al.* 2019). We employ it here to represent the streamwise-scale (λ_x) based linear coupling between z_o and z_r by considering u fluctuations acquired from the probes at these two locations, for various Δs, following

$$\gamma_L^2(z_o, z_r, \Delta s; \lambda_x) = \frac{|\langle \widetilde{u}(z_o, \Delta s; \lambda_x)\widetilde{u}^*(z_r; \lambda_x)\rangle|^2}{\langle|\widetilde{u}(z_o, \Delta s; \lambda_x)|^2\rangle\langle|\widetilde{u}(z_r; \lambda_x)|^2\rangle} = \frac{|\phi'_{u_o u_r}(z_o, z_r, \Delta s; \lambda_x)|^2}{\phi_{u_o u_o}(z_o, \Delta s; \lambda_x)\phi_{u_r u_r}(z_r; \lambda_x)}, \quad (4.1)$$

where $\tilde{u}(z_o, \Delta s; \lambda_x) = \mathcal{F}[u(z_o, \Delta s)]$ is the Fourier transform of $u(z_o, \Delta s)$ in either time or x depending on the data set. The asterisk ($*$), angle brackets ($\langle\,\rangle$) and vertical bars ($|\,|$) indicate the complex conjugate, ensemble averaging and modulus, respectively. Thus, $\phi'_{u_o u_r}$ is the one-dimensional cross-spectrum between $u(z_o, \Delta s)$ and $u(z_r)$, while $\phi_{u_o u_o}$ and $\phi_{u_r u_r}$ are the energy spectra at z_o and z_r, respectively. γ_L^2 may be interpreted as the spectral domain equivalent of a physical two-point correlation, and varies between $0 \leqslant \gamma_L^2 \leqslant 1$ owing to the normalization defined in (4.1).

Figure 2(*b*) plots the γ_L^2 contours for $z_o^+ \approx 2.6\sqrt{Re_\tau}$ and $3.9\sqrt{Re_\tau}$ for the $\mathcal{E}_1$ data set. Following Baars, Hutchins & Marusic (2016), we consider a coherence threshold of $\gamma_{filt}^2 = 0.05$ to identify a streamwise spectral cutoff $\lambda_{x,c}(z_o, z_r, \Delta s)$ to classify structures with $\lambda_x > \lambda_{x,c}(z_o, z_r, \Delta s)$ as being coherent between z_r and z_o for a specific Δs. As discussed in § 2, it is observed that an increase in Δs leads to reduction in the range of scales correlated between the two probes (that is, an increase in $\lambda_{x,c}$). While γ_{filt}^2 is used to identify relevant streamwise wavelengths, the spanwise offset between probes inherently filters out the possible range of spanwise wavelengths (λ_y) for coherent structures; that is, $\lambda_y > \lambda_{y,c}$, where $\lambda_{y,c}/\delta \sim 2(\Delta s/\delta)$ (this has been highlighted as $(\lambda_y/\delta)_{min}$ on the secondary y-axis in figure 2*b*). It implies that on increasing $\Delta s/\delta$, for example, to 0.1, only structures with $\lambda_x/\delta > 3.5$ and $\lambda_y/\delta > 0.2$ are correlated between the two probes. This means that these wall-attached structures, which are large both in length and span, have been isolated from the remaining assemblage of eddies. Hence, the corresponding cross-correlation should not be influenced by the smaller structures.

It is noted that γ_L^2 contours for the two cases of z_o tend to overlap at large $\Delta s/\delta$, suggesting that a similar range of large wall-attached structures (on an average) are correlated between probes at z_o and z_r, for any z_o lying in the log region (also observed by Baidya *et al.* 2019). Conclusions drawn from forthcoming discussions, focusing on these structures, are thus applicable across this region. Interestingly, figure 2(*b*) shows that superstructures ($\lambda_x/\delta > 10$; Hutchins & Marusic 2007) remain

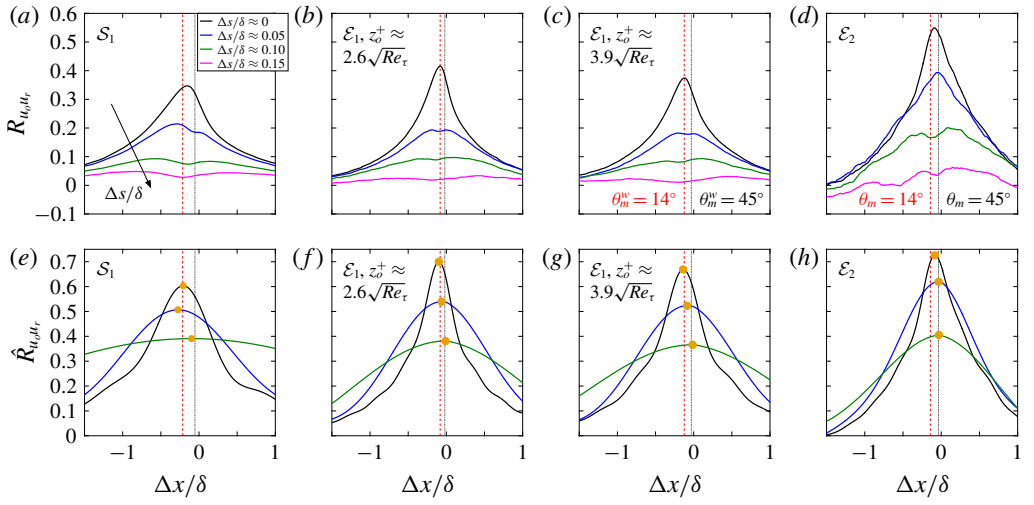

FIGURE 3. Cross-correlation of u measured at z_r and z_o, for various $\Delta s/\delta$, for data sets listed in table 2. (*a–d*) and (*e–h*) are correlations obtained from raw and large-wavelength-pass-filtered velocity time series, respectively, with a filter cutoff $\lambda_{x,c}(z_o, z_r, \Delta s)$ based on $\gamma_L^2(z_o, z_r, \Delta s) = 0.05$ computed for respective data sets. Red dashed and grey dot-dashed lines indicate $\Delta x/\delta$ corresponding to $\theta_m^w = 14°$ and 45°, respectively, for data sets $\mathcal{E}_1$ and $\mathcal{S}_1$, and $\theta_m = 14°$ and 45°, respectively, for data set $\mathcal{E}_2$. Here, $\theta_m = \text{atan}((z_o - z_r)/\Delta x_p)$. Yellow bullets in (*e–h*) highlight the peak in the cross-correlation.

correlated between the two probes up to $\Delta s/\delta \approx 0.14$. Such large structures, however, would be absent while analysing the data set $\mathcal{S}_1$ due to the limited streamwise domain ($\approx 11.9\delta$) considered.

4.2. *Variation of mean structure inclination angle with spanwise offset*

Having verified that large wall-attached structures are isolated on increasing Δs between probes at z_r and z_o, we now investigate the variation of θ_m (with Δs) by locating the peak (Marusic & Heuer 2007) in the correlation coefficient ($R_{u_o u_r}$) obtained on cross-correlating raw (unfiltered) velocity data from the two probes as follows:

$$R_{u_o u_r}(\Delta x, \Delta s) = \frac{\langle u(z_r; x, y) u(z_o; x + \Delta x, y + \Delta s)\rangle}{\sqrt{\langle u^2(z_r)\rangle}\sqrt{\langle u^2(z_o)\rangle}}; \tag{4.2}$$

$R_{u_o u_r}(\Delta x)$ for the three data sets, at selected Δs, is plotted in figure 3(*a–d*). It may be observed that the correlation curve changes from having a clear distinct peak at $\Delta s \approx 0$ to one exhibiting a bi-modal behaviour as Δs increases, for all data sets. The magnitude of the peak also drops significantly, making it difficult to locate a unique peak and associate it with the streamwise delay (Δx_p) corresponding to the inclination of the mean structure. It is interesting to note that one of these two peaks in $R_{u_o u_r}$ is consistently close to $\Delta x \sim 0$ for all the data sets. Since $\Delta x \sim 0$ corresponds to $\theta_m^w \sim 90°$, this peak may be associated with the randomly oriented structures (for example, isotropic structures), which are known (Alving *et al.* 1990) to bias the cross-correlation towards $\theta_m^w \sim 90°$ and negligibly contribute to the covariance (that is, the numerator in (4.2)). It is quite possible that some of these structures, which have no preferred inclination angle, may also be coherent across the two probes, apart from the

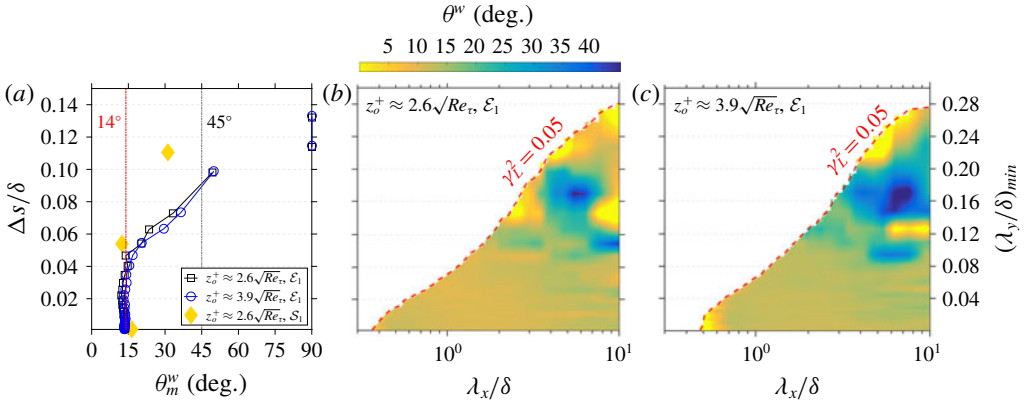

FIGURE 4. (*a*) Average structure inclination angle (θ_m^w) as a function of $\Delta s/\delta$ obtained by locating the peak of $\hat{R}_{u_o u_r}$ for data sets $\mathcal{E}_1$ and $\mathcal{S}_1$. (*b*,*c*) Scale-specific phase (Φ) of the cross-spectra ($\phi'_{u_o u_r}$), computed at various Δs, expressed as a physical inclination angle (θ^w) for $z_o^+ \approx$ (*b*) $2.6\sqrt{Re_\tau}$ and (*c*) $3.9\sqrt{Re_\tau}$ for data set $\mathcal{E}_1$.

majority forward-inclined structures (Perry *et al.* 1992). To make things clearer, the velocity data at both z_o and z_r are passed through a long-wavelength pass filter with a filter bound $\lambda_{x,c}(z_o, z_r, \Delta s)$ obtained from the corresponding $\gamma^2_{filt}(z_o, z_r, \Delta s) = 0.05$ for the three data sets (refer § 4.1). Application of this filter ensures that only those streamwise wavelengths are considered which have been stochastically found to be coherent between the two probes for various Δs (that is, wall-attached).

On filtering the velocity data, the new cross-correlation coefficient ($\hat{R}_{u_o u_r}$) is computed by replacing $u(z_o)$ and $u(z_r)$ with their filtered counterparts, $\hat{u}(z_o)$ and $\hat{u}(z_r)$ in (4.2), and is plotted in figure 3(*e–h*). Since $\lambda_{x,c}$ increases with Δs, $\hat{R}_{u_o u_r}$ becomes wider about the peak with increasing Δs. It is evident that the filtering aids in identification of a clear peak (highlighted by a yellow bullet) of the cross-correlation, with the associated correlation coefficient also having a significant value. The peak can be seen deviating from $\Delta x/\delta$ corresponding to $\theta_m = 14°$ (observed by Marusic & Heuer 2007) towards that for 45° with increasing Δs. This observation supports our hypothesis proposed in § 2 that $\theta_m \to \theta_s$ on increasing the spanwise offset between the two probes.

Here, θ_m^w obtained from $\hat{R}_{u_o u_r}$ for data sets $\mathcal{E}_1$ and $\mathcal{S}_1$, at various Δs, is plotted in figure 4(*a*). Indeed, θ_m^w increases from approximately 14° at $\Delta s \approx 0$ with increasing Δs, reaching close to 50° at $\Delta s/\delta \approx 0.1$, after which it jumps abruptly to 90° for larger offsets. This jump to 90° suggests that eddies with an inherent forward inclination do not span across such large offsets, and the coherence, $\gamma_L^2 \lesssim 0.1$, may be due to the randomly oriented eddies (Perry *et al.* 1992) co-existing in the TBL. These eddies tend to bias the cross-correlation peak towards $\Delta x \sim 0$ (Alving *et al.* 1990), which represents $\theta_m^w \sim 90°$ and has been observed in $R_{u_o u_r}$ plotted in figure 3. Taking this into consideration, the largest physically realistic values of θ_m^w are found to be approximately 35° and 50° at $\Delta s/\delta \approx 0.08$ and 0.10, respectively, which are both close to the theoretically supported angle of 45° (§ 1). This encourages us to conclude that θ_s^w is indeed nominally 45° for a large isolated flow structure. A similar trend of increasing θ_m^w, with increasing Δs, is also observed for the $\mathcal{S}_1$ data set (not shown completely for brevity), but the increment rate is relatively slow, probably

due to the limited streamwise scale range owing to the domain size selected for the analysis (discussed in § 4.1). Since the coherence becomes lower than the threshold ($\gamma_L^2 \lesssim 0.05$) across all λ_x for $\Delta s/\delta \gtrsim 0.15$, no cross-correlation (and θ_m) is obtained for such spans after filtering.

4.3. *Scale-specific inclination angle of wall-attached structures*

Analysing the cross-correlation yields θ_m, which is influenced by a range of scales (Marusic 2001). Since we see an increase in θ_m^w towards 45° with an increase in Δs (figure 4*a*), it would be interesting to see how a streamwise-scale-specific inclination angle ($\theta^w(\lambda_x)$) varies with Δs. Following Baars *et al.* (2016), θ^w is obtained from the scale-dependent phase information embedded in the cross-spectrum ($\phi'_{u_o u_r}$); $\phi'_{u_o u_r}(\Delta s;\, \lambda_x) = \mathcal{F}[R_{u_o u_r}(\Delta s;\, \Delta x)]$ has already been computed to find γ_L^2 in (4.1) and is complex-valued. The scale-specific phase (Φ) is estimated from $\phi'_{u_o u_r}$ as follows:

$$\Phi(\Delta s;\, \lambda_x) = \text{atan}\left\{\frac{\text{Im}[\phi'_{u_o u_r}(\Delta s;\, \lambda_x)]}{\text{Re}[\phi'_{u_o u_r}(\Delta s;\, \lambda_x)]}\right\}, \tag{4.3}$$

where Im and Re denote the imaginary and real components of $\phi'_{u_o u_r}$. We find Φ essentially records the shift of each Fourier mode, λ_x, owing to the correlation of u measured at two different wall-normal locations. A streamwise shift ($\ell(\Delta s;\, \lambda_x)$) is obtained from the phase (which is in radians) by pre-multiplying it with the respective Fourier mode – that is, $\ell(\Delta s;\, \lambda_x) = \lambda_x \Phi(\Delta s;\, \lambda_x)/(2\pi)$. A scale-specific physical inclination angle is then computed at each Δs following

$$\theta^w(\Delta s;\, \lambda_x) = \text{atan}\left\{\frac{(z_o - z_r)}{\ell(\Delta s;\, \lambda_x)}\right\}; \tag{4.4}$$

$\theta^w(\lambda_x,\, \Delta s)$ is plotted in figure 4(*b*) and (*c*) for $z_o^+ \approx 2.6\sqrt{Re_\tau}$ and $3.9\sqrt{Re_\tau}$, respectively, for data set $\mathcal{E}_1$. Here, we restrict our attention to streamwise wavelengths $\lambda_x/\delta \leqslant 10$ so that the interpretation of θ^w is not influenced by the assumption of Taylor's hypothesis (de Silva *et al.* 2015).

It can be seen in both figure 4(*b*,*c*) that θ^w, in general, increases with Δs and corresponds well with the variation of θ_m^w shown in figure 4(*a*). At $\Delta s \approx 0$, all the wall-coherent scales agree to an almost constant angle of $\theta^w \approx 14°$, even at large λ_x (Baars *et al.* 2016). This is because θ^w, here, is influenced by structures with $0 < \lambda_y < \infty$, meaning that not all the influencing structures are large in the two-dimensional sense. As $\Delta s/\delta > 0.04$, θ^w increases across all $\lambda_x > \lambda_{x,c}$ since only structures of spanwise wavelength $\lambda_y/\delta > 0.08$ influence the estimation. It is around this $\Delta s/\delta$ range where θ_m^w starts deviating from 14° (figure 4*a*). On increasing $\Delta s/\delta$ to 0.08, we are effectively considering only the large structures ($\lambda_x/\delta > 2$, $\lambda_y/\delta > 0.16$) for which $\theta^w \gtrsim 30°$, which aligns well with the previous estimations (θ_s; table 1) made via visualizing individual structures. It also explains the average estimation $\theta_m^w \approx 45°$ at similar offsets. The qualitatively similar variation of $\theta^w(\Delta s;\, \lambda_x)$ for both z_o^+, especially at high Δs (figure 4*b*,*c*), reinforces the fact that our conclusions should be applicable for all z_o^+ in the log region. It is difficult to physically interpret θ^w for $\Delta s/\delta > 0.11$ given that θ_m^w abruptly jumps to 90° for these offsets (figure 4*a*), suggesting a contribution from randomly oriented structures to the cross-correlation.

4.4. *Implications on LES and AEH-based simulations*

Having empirically established that $\theta_s^w \approx 45°$ (nominally) for isolated large wall-attached eddies, we now discuss possible implications of the findings of the present study on LES and AEH-based simulations. In recent AEH-based simulations (Baidya *et al.* 2014, 2017; Chandran *et al.* 2017), Λ-vortices organized in a packet are typically used as representative structures to statistically model the log region of a ZPG TBL. Simulation results reported by Marusic (2001) clearly indicate that the size and shape, as well as the orientation of the eddies, significantly influence the statistics yielded by the model. Over the years, researchers have attempted to improvise on the size and shape of the representative eddies (Marusic & Monty 2019), via trial and error, to mimic the experimental trends. However, in the case of the orientation of the individual eddies (θ_s^w), considering support from the theory (§ 1) as well as flow visualizations reported in the seminal studies of Head & Bandyopadhyay (1981) and others, θ_s^w has always been assumed to be nominally 45°. This trend has continued over the years without any concrete empirical evidence, which this study has attempted to address. Here, via physical and statistical filters, we have isolated the large wall-attached eddies and have empirically shown that θ_s^w is nominally 45° for these eddies, suggesting it to be a reasonable assumption for the orientation of the individual Λ-vortices considered for an AEH-based simulation.

Moving to the implication on LES simulations, due to limitations in computational power, high-Re_τ LES simulations typically only compute the outer layer of the TBL (Piomelli & Balaras 2002). The grid resolution for the simulation is thus chosen based on the outer layer eddies, making it incapable of resolving the relatively small eddies existing in the inner layer of the TBL, and in turn also limiting estimation of the wall shear stress (τ_w). In such a scenario, information from the computed outer flow is utilized to estimate τ_w (Marusic, Kunkel & Porte-Agel 2001), wherein the inclination of the elongated eddies in the inner layer needs to be accounted for. Earlier studies (Piomelli *et al.* 1989; Carper & Porte-Agel 2004) have used the experimentally obtained value of $\theta_m^w \approx 14°$ as the mean inclination of these eddies. However, the empirical observations in the present study (figure 4*a*) in conjunction with the simulations of Marusic (2001) strongly suggest that θ_m^w depends on the range of scales being considered in the flow. Since the inclination angle of solely the unresolved structures in the inner layer needs to be taken into account while estimating τ_w, θ_m^w for these selective range of scales may be a function of the grid resolution and consequently may differ from 14°.

5. Concluding remarks

The streamwise inclination angle of large wall-attached structures, in the log region of a TBL, is estimated statistically to be nominally 45°. This result was estimated by isolating these structures from the remaining assemblage of eddies by introducing a spanwise offset between the near-wall and log-region reference probe – a methodology which was shown to be effective for TBL data sets across $Re_\tau \sim O(10^3)$–$O(10^6)$. The angle obtained closely resembles the inclination of individual 'hairpin'-type structures considered to be the dominant feature of a wall-bounded turbulent flow (Moin & Kim 1985), suggesting wall-attached structures to be of similar type. The present findings also provide empirical evidence in support of the eddy inclination angles considered when simulating a TBL with AEH-based simulations. Although the empirical result, $\theta_s^w \approx 45°$, may be limited to large wall-attached structures, theoretical arguments discussed in § 1 give a strong indication of what the approximate θ_s^w of

relatively smaller wall-attached structures would be. The present findings may also have implications for the wall-layer models employed in high-Re_τ LES simulations of a TBL, which utilize experimentally determined θ_m^w to correlate wall shear stress with the velocity estimated at the near-wall grid point. The present analysis reveals that θ_m^w is a function of the range of scales considered for its estimation, and this range would vary with the grid size considered for the LES simulation.

Acknowledgements

The authors wish to acknowledge the Australian Research Council for financial support and appreciate the publicly available DNS data of Sillero *et al.* (2013).

References

ADRIAN, R. J., MEINHART, C. D. & TOMKINS, C. D. 2000 Vortex organization in the outer region of the turbulent boundary layer. *J. Fluid Mech.* **422**, 1–54.

ALVING, A. E., SMITS, A. J. & WATMUFF, J. H. 1990 Turbulent boundary layer relaxation from convex curvature. *J. Fluid Mech.* **211**, 529–556.

BAARS, W. J., HUTCHINS, N. & MARUSIC, I. 2016 Spectral stochastic estimation of high-Reynolds-number wall-bounded turbulence for a refined inner–outer interaction model. *Phys. Rev. Fluids* **1** (5), 054406.

BAARS, W. J., HUTCHINS, N. & MARUSIC, I. 2017 Self-similarity of wall-attached turbulence in boundary layers. *J. Fluid Mech.* **823**, R2.

BAIDYA, R., BAARS, W. J., ZIMMERMAN, S., SAMIE, M., HEARST, R. J., DOGAN, E., MASCOTELLI, L., ZHENG, X., BELLANI, G., TALAMELLI, A. *et al.* 2019 Simultaneous skin friction and velocity measurements in high Reynolds number pipe and boundary layer flows. *J. Fluid Mech.* **871**, 377–400.

BAIDYA, R., PHILIP, J., HUTCHINS, N., MONTY, J. P. & MARUSIC, I. 2017 Distance-from-the-wall scaling of turbulent motions in wall-bounded flows. *Phys. Fluids* **29** (2), 020712.

BAIDYA, R., PHILIP, J., MONTY, J. P., HUTCHINS, N. & MARUSIC, I. 2014 Comparisons of turbulence stresses from experiments against the attached eddy hypothesis in boundary layers. In *Proceedings of 19th Australasan Fluid Mechanics Conference, Melbourne, Australia*.

BROWN, G. L. & THOMAS, A. S. W. 1977 Large structure in a turbulent boundary layer. *Phys. Fluids* **20** (10), S243–S252.

CARPER, M. A. & PORTE-AGEL, F. 2004 The role of coherent structures in subfilter-scale dissipation of turbulence measured in the atmospheric surface layer. *J. Turbul.* **5**, 32–55.

CHANDRAN, D., BAIDYA, R., MONTY, J. P. & MARUSIC, I. 2017 Two-dimensional energy spectra in high-Reynolds-number turbulent boundary layers. *J. Fluid Mech.* **826**, R1.

HEAD, M. R. & BANDYOPADHYAY, P. 1981 New aspects of turbulent boundary-layer structure. *J. Fluid Mech.* **107**, 297–338.

HUTCHINS, N., CHAUHAN, K., MARUSIC, I., MONTY, J. & KLEWICKI, J. 2012 Towards reconciling the large-scale structure of turbulent boundary layers in the atmosphere and laboratory. *Boundary-Layer Meteorol.* **145** (2), 273–306.

HUTCHINS, N. & MARUSIC, I. 2007 Evidence of very long meandering features in the logarithmic region of turbulent boundary layers. *J. Fluid Mech.* **579**, 1–28.

JONES, M. B., MARUSIC, I. & PERRY, A. E. 2001 Evolution and structure of sink-flow turbulent boundary layers. *J. Fluid Mech.* **428**, 1–27.

MARUSIC, I. 2001 On the role of large-scale structures in wall turbulence. *Phys. Fluids* **13** (3), 735–743.

MARUSIC, I. & HEUER, W. D. C. 2007 Reynolds number invariance of the structure inclination angle in wall turbulence. *Phys. Rev. Lett.* **99** (11), 114504.

MARUSIC, I., KUNKEL, G. J. & PORTE-AGEL, F. 2001 Experimental study of wall boundary conditions for large-eddy simulation. *J. Fluid Mech.* **446**, 309–320.

MARUSIC, I. & MONTY, J. P. 2019 Attached eddy model of wall turbulence. *Annu. Rev. Fluid Mech.* **51**, 49–74.

MOIN, P. & KIM, J. 1985 The structure of the vorticity field in turbulent channel flow. Part 1. Analysis of instantaneous fields and statistical correlations. *J. Fluid Mech.* **155**, 441–464.

PERRY, A. E. & MARUSIC, I. 1995 A wall-wake model for the turbulence structure of boundary layers. Part 1. Extension of the attached eddy hypothesis. *J. Fluid Mech.* **298**, 361–388.

PERRY, A. E., UDDIN, A. K. M. & MARUSIC, I. 1992 An experimental and computational study on the orientation of attached eddies in turbulent boundary layers. In *Proceedings of the 11th Australasian Fluid Mechanics Conference, Hobart, Australia*.

PIOMELLI, U. & BALARAS, E. 2002 Wall-layer models for large-eddy simulations. *Annu. Rev. Fluid Mech.* **34** (1), 349–374.

PIOMELLI, U., FERZIGER, J., MOIN, P. & KIM, J. 1989 New approximate boundary conditions for large eddy simulations of wall-bounded flows. *Phys. Fluids* A **1** (6), 1061–1068.

ROBINSON, S. K. 1991 Coherent motions in the turbulent boundary layer. *Annu. Rev. Fluid Mech.* **23** (1), 601–639.

SILLERO, J. A., JIMÉNEZ, J. & MOSER, R. D. 2013 One-point statistics for turbulent wall-bounded flows at Reynolds numbers up to $\delta^+ \approx 2000$. *Phys. Fluids* **25** (10), 105102.

DE SILVA, C. M., SQUIRE, D. T., HUTCHINS, N. & MARUSIC, I. 2015 Towards capturing large scale coherent structures in boundary layers using particle image velocimetry. In *Proceedings of the 7th Australian Conference on Laser Diagnostics in Fluid Mechanics and Combustion, Melbourne, Australia.*

UDDIN, A. K. M. 1994 The structure of a turbulent boundary layer. PhD thesis, University of Melbourne.